ADVANCED FUNCTIONAL MATERIALS
www.afm-journal.de

Contact-Driven Snapping in Thermally Actuated Metamaterials for Fully Reversible Functionality

*Ruizhe Ma, Lei Wu, and Damiano Pasini**

Mechanical instability is often harnessed in mechanical metamaterials to generate a diverse range of functionalities, and can be triggered by either a mechanical or a field stimulus, such as temperature. Existing field-responsive metamaterials with snap-through instability, however, need to rely on a mechanical input to realize functional reversibility, a limitation depriving them of the capacity to operate solely via the applied field. This work demonstrates reversible snap-through instability in a bi-material framework that is exclusively driven by environmental temperature. The need for mechanical intervention is bypassed by leveraging the thermally induced contact and mismatched thermal expansion of the constituent materials. A combination of experiments, theory and simulations, unveils the physics underpinning the thermally driven snapping undergoing four successive regimes of deformation: noncontact, full contact, partial contact, and release. The advantages of the concept are showcased in two applications. The first is the development of thermal switches with ternary operation (OFF-ON-OFF) and logic functions, going beyond the capabilities of current binary switches. The second is reversible temporal morphing in deployable structures programmed to snap sequentially in multiple locked configurations at predefined values of temperature, opening the door to applications across sectors, such as deployable antennas, soft robots, and self-reconfigurable medical devices.

1. Introduction

Metamaterials that shape morph in response to a mechanical input or an environmental stimulus have been demonstrated to hold remarkable promise for a large palette of applications across disciplines. Fast actuation speed, tunable large deformation, and output power amplification are appealing functional responses that shape morphing metamaterials can often attain by leveraging mechanical instabilities in soft actuators,[1–3] logic gates,[4,5] and soft robots,[6,7] among others. The occurrence of a mechanical instability indicates that a system rapidly transitions from one equilibrium state to another, a phenomenon that can result in a sudden and sizeable change in deformation. Whereas for a monostable elastic system, the deformation is recovered upon load removal thus bringing the system to its original state, for a bistable system, snap-through instability can generate bouncing between two stable states, each associated with a distinct configuration. If more bistable elements are stacked in series or parallel, the material system can undergo multiple stable states.[8]

Both buckling instability and snap-through instability have been extensively used to generate shape morphing in soft metamaterials.[9] A classic example of the former is the sudden pattern transformation of a planar cellular elastomer that undergoes buckling instability.[10,11] Other examples leveraging buckling instability for spatial shape morphing include 3D mesostructures tethered to a pre-stretched elastic substrate,[12,13] and elastic shells patterned with circular voids under pneumatic actuation.[14] Snap-through instability, on the other hand, has been exploited in bistable metamaterials to generate rapid alternation of equilibrium states. Notable examples, among others, include the attainment of both auxeticity and bistability into a planar sheet of rubber kirigami excised with geometric motifs of three and four-fold rotational symmetry,[15] and the sequential shape morphing induced by multistability in reconfigurable metamaterials consisting of multiple bistable units.[8,16,17] All the concepts reported above rely on the application of a mechanical input to trigger either buckling or/and snap-through instability. While effective, this strategy limits their capacity to rely only on the environment to operate. Rather it requires the integration of other functional devices, such as valves, sensors, motors, and controllers, disadvantages that also yield a substantial increase of weight, a reduction of the degrees of freedom, and a severe limitation to work in remote places.

Stimuli-responsive materials, on the other hand, have the potential to address such challenges. Shape memory polymers (SMPs),[18–20] hydrogels,[21–23] liquid crystal polymers (LCPs),[24,25] and dielectric elastomers (DEs),[26] can respond to a change in an environmental stimulus, such as temperature, without relying on the application of an external force. There are several mechanical metamaterials that harness stimulus responsive materials and mechanical instability. All of them, however, require both the exposure to a stimulus and the application of a mechanical input to operate; none of them can function through the sole exposure to an environmental

R. Ma, L. Wu, D. Pasini
Department of Mechanical Engineering
McGill University
Montreal, Quebec H3A 0C3, Canada
E-mail: damiano.pasini@mcgill.ca

The ORCID identification number(s) for the author(s) of this article can be found under https://doi.org/10.1002/adfm.202213371.

DOI: 10.1002/adfm.202213371

cue. For example, bistable elements made of SMP, have been used to propel the action of paddles in swimming robots pre-programmed to perform prescribed tasks in water. After each propulsion, however, a mechanical force is needed to reset the bistable elements to their pre-snapping state in charge of delivering the next locomotion step.[27] Hydrogels and polydimethylsiloxane (PDMS) have been used to embody logic in an assembly of bistable elements capable of swelling anisotropically in response to multiple stimuli. However to transition to their second stable state, the laterally-confined, unstrained beams need to be exposed to a mechanical load.[28] Another example pertains to the use of a thermomechanical cycle to replicate shape memory behavior in a snapping metamaterials, where again the transition to the second stable state is triggered by an external mechanical load, while the temperature variation drives back the metamaterial to its initial state.[29] All existing concepts rely on mechanical intervention to switch to their second stable state so as to activate the snap-through capacity,[27–29] hence showing their inability to operate solely by means of an environmental cue.

In this work, we demonstrate the emergence of reversible snap-through instability that is entirely temperature-actuated, eliminating the need for any mechanical intervention. We introduce a metamaterial architecture that leverages thermally induced contact to trigger snapping during a temperature increase, ΔT, with respect to room temperature. The architecture in the post snap-through state is capable of resuming its original configuration when the temperature returns to the initial value, allowing for a reversible transformation. The concept consists of two outer rigid frames, each with a centrally shaped protrusion, namely a stopper, that clamp an inner soft core. The constituent materials have a distinct coefficient of thermal expansion (CTE), and their thermal mismatch in volumetric expansion enables the metamaterial to go through four sequential regimes: noncontact, full contact, partial contact, and release. We first unveil the existence of two critical regimes of temperature, i.e., $\Delta T_{contact}$, the change of temperature required to achieve full contact, and ΔT_{snap} triggering snapping, and then showcase how to leverage the newly defined temperature regimes into two distinct applications. The first is the design of a ternary thermal switch where we exploit the contact-release mechanism, and the second entails the sequential deployment of specified modules in a deployable structure that benefits from the high tunability of ΔT_{snap} regime.

2. The Physical Mechanism of Contact-Induced Snapping under Temperature

2.1. Contact-Induced Snapping Unit Cell

Figure 1a illustrates our thermal snapping unit made of multimaterial constituents that undergo dimensional changes and contact in response to a varying temperature. The unit architecture consists of an expanding core with high CTE and two stiff restraining frames with low CTE arranged in a symmetric pattern. The former features two horizontal beams with semi-elliptical grooves connected by a central pillar, while the latter are shaped along each horizontal median with stoppers, i.e., rectangular protrusions. The stoppers regulate the internal contact mechanism and the thermally induced snapping. They are the enabler of a shape transformation that is entirely temperature-actuated and reversible, functionalities that extend those of existing stimulus responsive metamaterials harnessing mechanical instability.

In the undeformed state (Figure 1a(i)), the core and the stoppers do not interact, and a gap separates their opposing surfaces. As the temperature increases, the constituent volumes expand at a rate controlled by the value of their own CTE. The CTE mismatch between the two first yields the narrowing and closure of the gap (Figure 1a(ii)). Following the establishment of full contact, the stoppers impede downward displacement and divert the internal motion in the opposite direction (Figure 1a(iii)) until thermal snapping takes place (Figure 1a(iv)). We can identify four emerging regimes governed by temperature (Figure 1b), each pertinent to specific characteristics entailing contact modality and deformation mechanism; we describe them by assessing the global displacement and CTE response of the unit cell. Here, the CTE is defined as $(h - h_1)h_1^{-1}\Delta T^{-1}$, where h denotes the global height of the unit cell in a given deformed state and h_1 denotes the unit cell height in the undeformed state. In the first regime (gap reduction), the height of unit cell decreases from h_1 to h_2, resulting in a negative CTE value. In the second regime of (full contact), the displacement remains negative until the central portion of the contact area separates and the CTE remains negative but with a decline in absolute magnitude. In the third regime (partial contact), the middle portion of the core separates from the stoppers, converting the prior full contact to partial contact. The shift in deformation mode causes a change in the displacement curve and CTE, the latter transitioning from negative to positive during the partial contact stage, where $h_3 > h_1$. Finally, snap-through instability in the fourth regime (full release) occurs, causing an abrupt loss of contact and the full release of the upper part of the frame, a phenomenon that produces a large displacement in response to a tiny increment of temperature. In the final stage of full release, we observe a sharp uprise of the CTE reflecting a large increase of displacement upon a narrow temperature range. The CTE, which measures the fractional change in dimension per degree change in temperature, decreases afterward, even when the unit height continues to rise.

During a full cycle of temperature, our unit can store and release energy upon heating as well as return to its initial state by undergoing hysteretic behavior upon cooling. This is shown in Figure 1c through a three-dimensional plot of the strain energy versus displacement and ΔT, with the red arrow representing the snap open deformation and the blue arrow representing the snap back deformation. The strain energy initially increases because of heating across the first three regimes before dropping at the instant of snapping.[30] Here at $\Delta T = 42$ °C, a portion of the stored energy is released from state iii) to state iv) during the heating process (Figure 1c (2D inset)) to drive the unit cell from partial contact to full release. In the fourth regime, a further increase of temperature results in an additional store of the strain energy. Upon cooling down to the initial temperature, our unit snaps back to its initial state without any mechanical intervention, resulting in a significant displacement change (blue arrow).

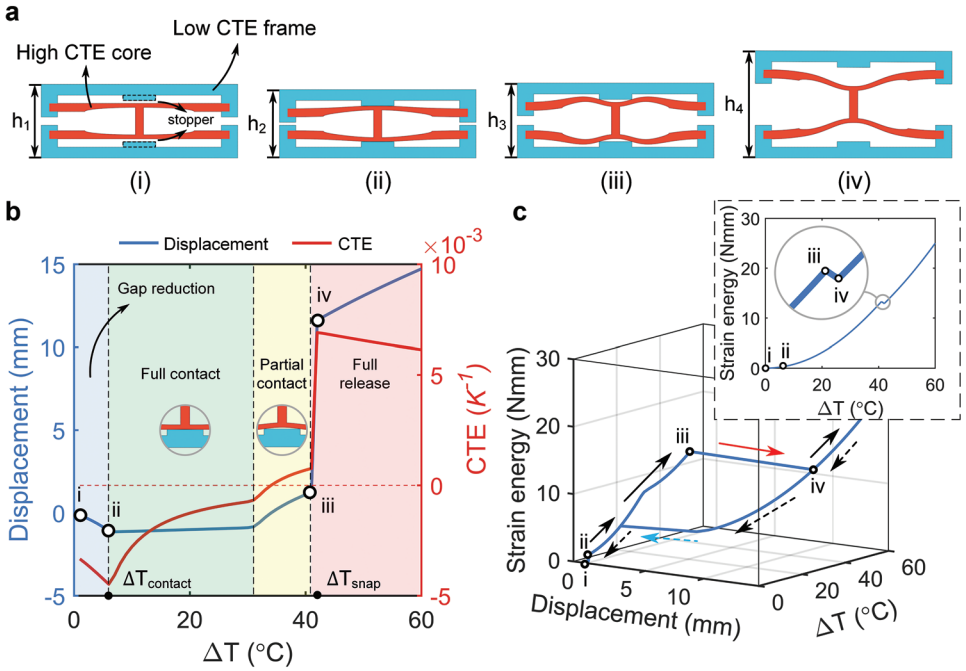

Figure 1. Thermally induced contact in responsive unit cell undergoing thermal snapping. a) Unit cell composed of a high CTE flexible core and two low CTE stiff frames forming gaps between them in the undeformed state i). Upon heating, the gap reduces and the core comes into full contact with the stoppers [full-contact-state ii)]. As the temperature rises, the central part of the core separates from the stoppers, shifting from full to partial contact [state iii)]. Upon a tiny temperature variation, the unit jumps to state iv) through snap-through instability. Throughout the process, the unit height decreases from h_1 to h_2, reducing the internal gap, followed by an increase of the unit height to h_3 caused by the contact with the stoppers. A substantial increase from h_3 to h_4 is produced by snapping. b) Plots of displacement and CTE against temperature change ΔT. From left to right the domain consists of four regimes: gap reduction, full contact, partial contact, and full release. Contact and snap temperature changes are denoted as $\Delta T_{contact}$ and ΔT_{snap}. c) Plot of strain energy against displacement and ΔT illustrating an energy drop from state iii) to state iv) when snapping happens, and exhibiting reversible morphing of a unit cell throughout a heating and cooling cycle. The unit returns to its original state i) when the temperature is lowered to the initial value. The red arrow represents the snap open deformation and the blue arrow represents the snap back deformation. The 2D inset depicts the change in strain energy during the heating process.

2.2. Unveiling the Interplay between Thermally Induced Contact and Snapping

To better elucidate the thermally actuated snapping behavior that brings the unit from partial contact to full release, we develop a simple yet effective spring-mass model that captures the physics of the phenomenon that underpin this work and extend the capabilities of existing concepts. For the sake of symmetry, we examine a quarter of the unit with gap equal to zero, and simplify its physical layout by removing the connecting pillar between the upper and lower part of the core (**Figure 2**a(i), top). The result is a structural analog composed of two elastic linear springs with constants k_1 and k_2 pinned together, with the left end (point A) simply supported, the middle (point B) impeding downward translation due to the stopper, and the right (point C) free to move vertically (Figure 2a(i), middle). Rotation is restrained at points A,B,and C by three rotational springs with constants β_1, β_2 and β_3 ($\beta_3 = \beta_2$). The system has two degrees of freedom characterized by the angular displacements θ_1 and θ_2 that generate the deformed state superimposed to its undeformed counterpart (Figure 2a(i), bottom). The length change of the spring, Δl, during heating is caused by two factors: 1) the elongation owing to the thermal expansion and 2) the contraction due to the axial force. This relation can be expressed as follows

$$\Delta l = \Delta l_{\text{expansion}} - \Delta l_{\text{compression}} \tag{1}$$

where $\Delta l_{\text{expansion}}$ and $\Delta l_{\text{compression}}$ can be calculated through the skew angles θ_1,θ_2, initial values of θ_1^*,θ_2^*, heights h_l, h_r, length l, spring stiffness k_1, k_2, CTEs α_1, α_2, temperature change ΔT, and reaction forces P and R. This yields the following for Δl_{AB} and Δl_{BC}

$$\Delta l_{\text{AB}} = h_l\left(\frac{1}{\sin\theta_1} - \frac{1}{\sin\theta_1^*}\right) = \frac{h_l}{\sin\theta_1^*}\alpha_1\Delta T - \frac{1}{k_1}\left(P\cos\theta_1 + R\sin\theta_1\right) \tag{2}$$

$$\Delta l_{\text{BC}} = \frac{l - \frac{h_l}{\tan\theta_1}}{\cos\theta_2} - \frac{h_r}{\sin\theta_2^*} = \frac{h_r}{\sin\theta_2^*}\alpha_2\Delta T - \frac{P\cos\theta_2}{k_2} \tag{3}$$

Considering the moment equilibrium of AB and the entire system, and taking moments about points A and C, respectively, we can obtain

$$M_1 + Ph_l - M_2 - R\frac{h_l}{\tan\theta_1} = 0 \tag{4}$$

$$M_1 + R\left(l - \frac{h_l}{\tan\theta_1}\right) + P\left[h_l - \left(l - \frac{h_l}{\tan\theta_1}\right)\tan\theta_2\right] - Rl - M_3 = 0 \tag{5}$$

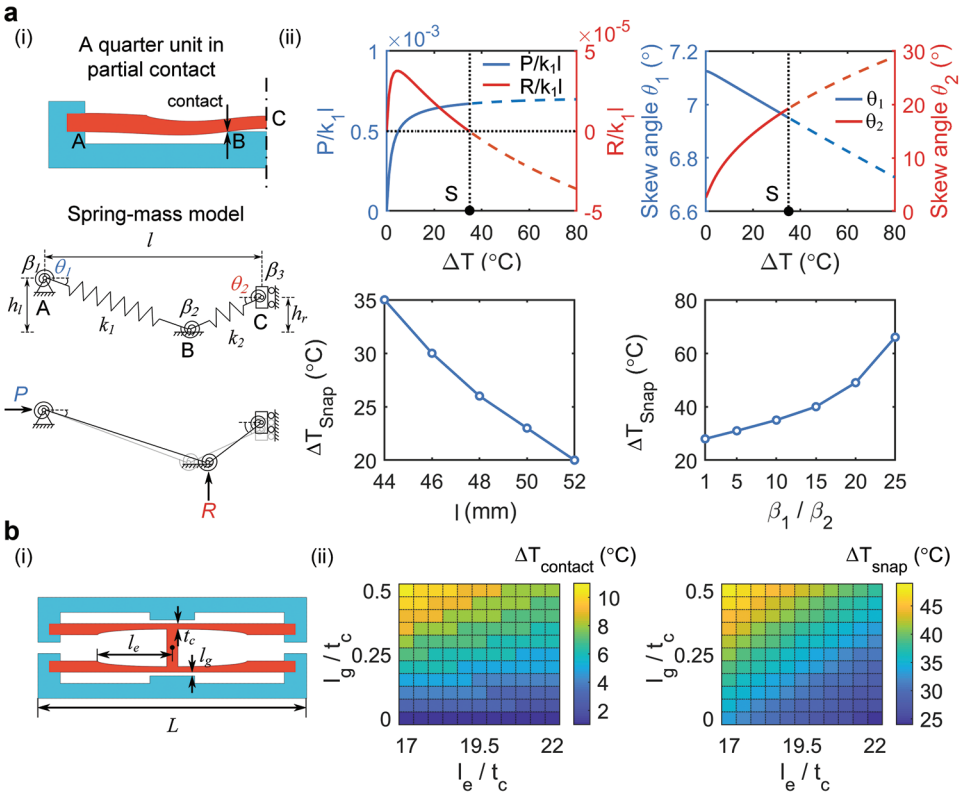

Figure 2. Analyses for a two-degree-of-freedom spring system and role of geometric attributes in the thermal responses of the unit cell. a) i) Reduced model for snapping unit analysis, where a quarter of the unit is examined when subjected to a temperature change, ΔT. The deformed state is superimposed with the undeformed state using bars for visual purpose. ii) Top graphs of temperature-induced normalized forces P/k_1l and R/k_1l and deformations θ_1 and θ_2 versus ΔT for given $l = 44$ mm and $\beta_1/\beta_2 = 10$. The onset of snapping can be identified by the intersection point of the R/k_1l -curve and the zero-force axis. Data sets after snapping do not actually exist and are depicted by dashed lines. ii) Bottom graphs of ΔT_{snap} versus l and β_1/β_2 ($\beta_2 = \beta_3$). b) i) Geometric characterization of the unit and ii) achievable ranges of contact temperature change $\Delta T_{contact}$ and snap temperature change ΔT_{snap} measured in prescribed spectrums of l_e/t_c and l_g/t_c.

where the moments M_1,M_2,M_3, can be calculated through the rotational spring stiffness and angular displacement.

By numerically solving the four equations (Equation 2–5) via the Newton's method, we find the roots for P,R,θ_1,θ_2 and plot the skew angles and the forces normalized by k_1l with respect to ΔT for given parameters h_l,h_r,l and physical quantities k_1/k_2,β_1/β_2 (Figure 2a(ii), top). The plots illustrate that during heating, R/k_1l (red curve representing the action of the stoppers) initially raises, but ultimately decreases and becomes negative, whereas P/k_1l (blue curve) always remains positive. With regard to the skew angles, θ_1 decreases as opposed to θ_2 which increases throughout the heating process. The insights gained from this analysis unveil that the stoppers initially provide upward support (i.e., positive reaction force R) once the thermally induced contact is established and the full contact state changes to partial contact. Above a critical temperature change S, however, R becomes negative, a value representing a downward (pull back) force that the stoppers cannot generate. As a result, snapping takes place at the point where R transitions from a positive to a negative value. Given the solutions after snapping ($R = 0$) are only theoretical, we plot them as dashed lines.

Additional insights we draw from this analysis pertain to the role that the length l and rotational stiffness ratio, β_1/β_2, of the unit cell play on ΔT_{snap}. Figure 2a(ii), (bottom) shows the plots of both parameters controlling the response of the spring model. An increase in l lowers $\Delta T_{snap,}$ indicating that a milder increase in temperature is required to trigger the snapping of a longer unit. In contrast, a more constrained rotation at point A, described by a larger ratio of rotational spring stiffness, β_1/β_2, requires a larger temperature increase to achieve snapping. For example, increasing l from 44 to 52 mm generates a 42.9% reduction (35 °C to 20 °C) in ΔT_{snap}, while an increment of β_1/β_2 from 1 to 25 results in a 135.7% gain (28 °C to 66 °C) in ΔT_{snap}. Supporting Information Section S2 includes the details of the analysis with additional information on the geometric parameters,physical quantities, and equilibrium equations of the spring model.

2.3. Role of Geometric Attributes in Governing Unit Cell Response

Under a change in temperature, our contact-induced snapping unit exhibits contact and snap at $\Delta T_{contact}$ and ΔT_{snap}, respectively, values that are governed and can be tuned by its geometric attributes. Among all the geometric parameters defining our unit cell (see Section S1, Supporting Information),

we focus here on the elliptical groove length, l_e, gap distance, l_g, and core thickness, t_c, that most influence the unit response (Figure 2b(i)). For a given pair of CTEs for the core (α_c) and frame (α_f), the attainable ranges of $\Delta T_{contact}$ and ΔT_{snap} are mapped with respect to l_e and l_g, normalized by a prescribed t_c. The trends in Figure 2b(ii) show that the larger l_g/t_c, the higher $\Delta T_{contact}$ and ΔT_{snap}, whereas the greater l_e/t_c, the lower the responses, a result that is consistent with those in Figure 2a(ii). For example, $\Delta T_{contact}$ and ΔT_{snap} increase from 0 °C, 33 °C to 11 °C, 49 °C, respectively, when l_g/t_c raises from 0 to 0.5 at constant $l_e/t_c = 17$. On the other hand, $\Delta T_{contact}$ and ΔT_{snap} drop from 11°C,49 °C to 8 °C,38 °C, respectively, when l_e/t_c increases from 17 to 22 at $l_g/t_c = 0.5$. In general, as the unit length increases (decreases) and the gap narrows (widens), the temperature change needed to achieve contact and snap decreases (increases). Movie S1 (Supporting Information) demonstrates that two units with tailored geometries can snap at distinct temperatures and exhibit reversible deformation upon heating and cooling.

3. Development of Ternary Thermal Switch with Logic Functions

We now leverage the contact-release mechanism and the thermal snapping regimes of our unit to showcase the development of a thermal switch with OFF-ON-OFF operation and logic functions. Current switches connect/disconnect circuits by switching states between OFF and ON, and can be divided into two categories: active and passive switches. The former require an external input information (e.g., voltage) to transition between a closed and open state,[31] whereas the latter are triggered in response to environment cues with no energy consumption.[32,33]

Passive switches are binary, i.e., have two states only, and upon a rise in temperature can turn on the circuit, i.e., from OFF to ON, and maintain that state. Here, we present a ternary thermal switch with three consecutive states: OFF-ON-OFF, an operation that could be attained only by employing a set of binary switches. Our ternary switch, on the other hand, upon a rise in temperature can switch the circuit back to OFF after the previous ON state, i.e., from OFF to ON and then OFF again. The additional OFF state that follows the ON state is advantageous over current binary switches because it provides a second temperature threshold, above which the circuit is empowered to be automatically cut off. This additional threshold cannot be provided by current binary switches which could offer one single temperature threshold.

For the thermal switch demonstration, we first develop a fabrication process to realize bi-material snapping units comprising off-the-shelf materials and to enable the separate fabrication and subsequent assembly of the cores and frames, hence relaxing the reliance of current manufacturing strategies on material chemistry and process parameter tuning (**Figure 3**a). For our proof-of-concept fabrication, we select two representative materials: silicone rubber (high CTE) and wood (low CTE). First, a mold is 3D printed using polylactic acid (PLA) (ANYCUBIC Vyper). A two-part silicone rubber (SILPAK R-2374A/B) is then mixed, injected into the void, and demolded once fully cured. Next, two frames are laser cut (SignCut CM1290) out of a wood panel. The components are then assembled and bonded together with epoxy glue (Adhaer 5 Min Epoxy) to ensure strong adhesion. To enable insulated materials to be employed as a switch in an electrical circuit, 0.1 mm thick copper tapes are affixed to the core and stoppers, and wired to a circuit containing a light bulb. By identifying the OFF or ON state of the bulb, we can assess the (noncontact/contact) interaction between core and stoppers, and hence measure the corresponding temperature changes, $\Delta T_{contact}$ and ΔT_{snap}.

The left side of Figure 3b depicts the responses of our unit cell with varying l_e/t_c at a prescribed gap distance l_g, demonstrating the switch capability to regulate circuit connection and disconnection at distinct values of temperature. The domain is divided into three sub-domains, OFF,ON, and OFF, whose boundaries are defined by the contact (blue) and snap (red) curves. The right hand side of Figure 3b shows an experimental illustration of the thermal switch with OFF-ON-OFF operation. For $\Delta T < \Delta T_{contact}$, the light bulb remains OFF because the core and stoppers have not made contact yet. For $\Delta T_{contact} \leq \Delta T < \Delta T_{snap}$, the contact is established, the switch turns on, and the bulb lights up. Snapping takes place when $\Delta T = \Delta T_{snap}$, leading to the separation of the core from the stoppers, thus cutting off the circuit. The experimental measurements of $\Delta T_{contact}$ and ΔT_{snap} are plotted with respect to l_e/t_c, showing quantitative agreement with the computational results. The lower and upper temperature boundaries of the ternary switch have a twofold benefit over existing binary switches. First the circuit can operate within a specific service temperature span that is bounded from both sides of the range. Second, the switch can be autonomously reset when the temperature returns to room temperature.

An additional functionality of our ternary switch is that by setting the gap to null, i.e., $l_g = 0$ (Figure 2b(i)), we can degrade it to a binary one, where the core and stoppers are in full contact in the undeformed state. This versatility enables our metamaterials to operate as either ternary or binary switch. For binary operations, we can embed logic functions by integrating multiple binary snapping units with varying ΔT_{snap}. An input signal element is a snapping unit, whose logic state is defined as 0 or 1, as determined by the unit configuration, either contact or release. On the other hand, an output signal element is a light bulb, whose OFF or ON state determines the output of 0 or 1 (**Figure 4**(i)).

We now demonstrate the attainment of a range of logical operations by connecting individual unit cells in given configurations. First, a NOT function is realized by connecting an input and output element in series (Figure 4(ii)). The logic state of the input signal element is 0 when $\Delta T < \Delta T_{snap}$, resulting in an output signal of 1. When $\Delta T \geq \Delta T_{snap}$, the input element snaps to logic state 1 and the output switches from 1 to 0. The output can also be determined by several inputs, giving rise to three other logical functions OR,NOR,and AND, where two input signal elements are connected either in parallel, series or combination thereof, and can be programmed to switch logic state at distinct temperatures due to the tunability of ΔT_{snap}. For example, consider the OR function; two inputs are connected in series and then in parallel with the output, which can switch from 0 to 1, when at least one of the input elements snaps to

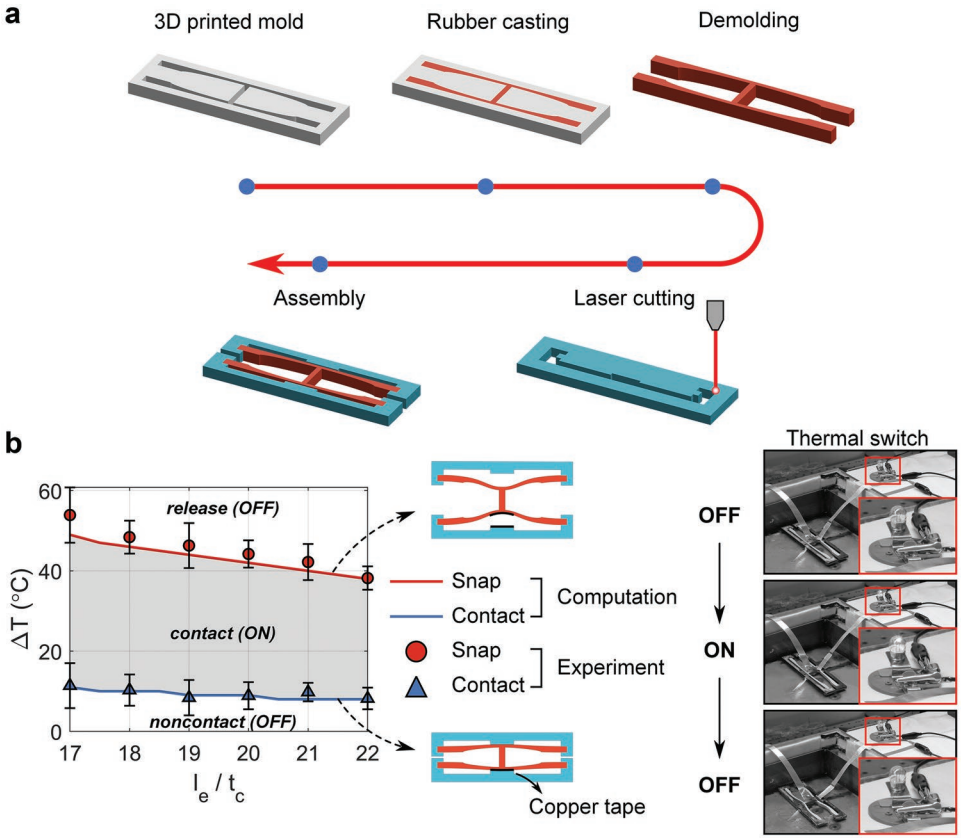

Figure 3. Fabrication of bi-material snapping unit and its application as thermal switch. a) Core and frame manufactured separately and assembled thereafter. The former is made of silicone rubber obtained by casting the liquid compound in a 3D printed PLA mold with a core shaped void, while the latter is laser cut out of a wood panel. Two components are assembled and bonded together with epoxy glue to ensure a sturdy connection. b) OFF-ON-OFF thermal switch enabled by contact-induced snapping unit. The unit responses, $\Delta T_{contact}$ and ΔT_{snap}, are plotted with respect to the normalized elliptical groove length, l_e/t_c, with experimental results overlaid on computational ones. The domain is divided into three sub-domains by the curve contact (blue) and snap (red). An experimental demonstration of a thermal switch with OFF-ON-OFF operation is displayed. Samples are tested in water bath.

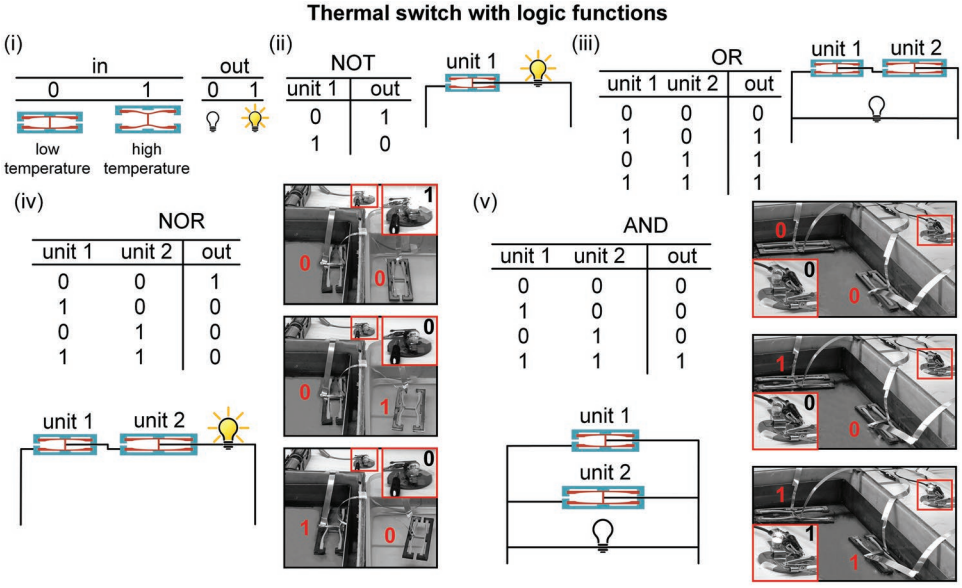

Figure 4. Thermal switch with logic functions. i) Logic state of input and output signal elements. ii)–v) Four logic functions NOT,OR,NOR, and AND created by incorporating one or two input elements in parallel, series, or combination thereof. Truth tables of the four logics and experimental validations for NOR and AND are included.

logic state 1 (Figure 4(iii)). Under identical input conditions, on the other hand, the output of NOR logic, which connects inputs and output in series, can shift from 1 to 0 (Figure 4(iv)). Moreover, to flip the AND output from 0 to 1, both logic inputs must be switched from 0 to 1 (Figure 4(v)). Thermal experiments demonstrate the achievement of NOR and AND logics using input elements, ΔT_{snap} = 24 °C and ΔT_{snap} = 33 °C. The experimental outcomes are consistent with the corresponding truth tables.

The advantage of using a thermal switch with embedded logic functions can be capitalized in scenarios where we need to monitor temperature values from multiple independent environments to ensure that the output element, which can be a delicate and sensitive equipment, operates within the service temperature range. By virtue of the interplay between the thermally induced contact and snap behavior of our units, the switch does not require any additional sensors, controllers, or actuators. For instance, if the monitored temperature exceeds a given threshold, an automatic cutoff can be performed by a circuit utilizing a thermal switch with NOT function. By employing a thermal switch with NOR function, the equipment in the circuit operates only if two monitored environmental temperatures are below specified levels. If either exceeds the threshold, the circuit will be cut off to protect equipment from overheating. In addition to preventing overheat through automated cutoff, a thermal switch with inbuilt function can be used to regulate the equipment to start operating once the environmental requirements are met. For example, a thermal switch with AND function can turn on the circuit if and only if the criteria for the two ambient temperatures are concurrently fulfilled. In another scenario, if one of the two monitored environmental temperatures fulfills the service criteria, the circuit can be engaged using the OR function switch. More input elements can be incorporated to generate more complex operations, such as to sense and respond to temperatures from numerous fields and achieve more sophisticated control. In addition, the thermal switches endowed with logic functions are ideal for applications that demand repeated thermal cycles by virtue of their reversibility, which allows the switches to reset when the temperature returns to the initial value.

4. Demonstration of Thermally Actuated Temporal Deployment

While previous section demonstrates the realization of thermal switches with logic functions through the integration of one or two unit cells, here, we focus on the collective behavior of a larger ensemble of unit cells. The goal is to demonstrate that a finite structure can sequentially deploy and lock into distinct configurations, each attained at a given temperature. Two factors come together to accomplish the sequential deployment: 1) the encoded snapping deformation concealed during heating by thermally induced contact, and 2) the large deformation created by thermally induced snapping. Both characteristics reduce the requirement for bulky hydraulic or pneumatic systems as well as for the addition of mechanical systems that are used to lock the deployment of selected components.

By carefully tailoring the geometry and spatial arrangement of the individual units, we can program the temporal sequence of deployment events over time. Several strategies have been studied in the literature to achieve temporal morphing, such as the local application of the stimulus,[34,35] the use of differential material diffusion rates upon exposure to a global stimulus,[36,37] and the local programming of material properties.[20,38] Nevertheless, most temporal morphing concepts are limited to irreversible self-folding, and primarily require manipulation of material chemistry, such as programming the transition temperature of SMP, and/or rely on changes in the applied stimuli, such as stimulus location. Here, we leverage the mechanism of contact-induced thermal snapping not to only perform linear and rotational morphing with reversibility, but also to control the sequence of deformations without relying on any manipulation of the external stimulus and merely resorting to off-the-shelf materials.

We first expand upon the linear deformation to introduce a rotational deformation mode by breaking the unit symmetry. Specially, we add a connector to constrain the relative deformation between points A,C or B and D, such that the resulting unit cell can show distinct rotation when snapping takes place (**Figure 5**a). A counterclockwise rotation snapping can be attained upon heating by connecting the left portion of the core. To program ΔT_{snap} of the rotational units and tessellate them as a whole with uniform frame dimension L, we prescribe L and tailor t_c, the parameter of the core thickness. Figure 5b depicts a nearly linear relationship between ΔT_{snap} (from 26 °C to 45 °C) and t_c, with a slight divergence attributed to the highly nonlinear nature of the contact behavior between core and stoppers. By introducing the rotational unit and exploring its achievable range of ΔT_{snap}, temporal morphing with rich geometric diversity can be obtained.

Next, we expand upon the unit cell to demonstrate the collective deployment of an ensemble of units capable of deploying sequentially in local regions at distinct values of the snapping temperature (Figure 5c). We develop a 1D non-periodic deployable structure composed of a sequence of twenty rotational units with t_c = 2 mm, ΔT_{1snap} = 26 °C and t_c = 3 mm, ΔT_{2snap} = 45 °C. In particular, six units with lower ΔT_{1snap} are connected to seven units with higher ΔT_{2snap} on each side, which rotate in the opposite direction. When the temperature is raised from the initial value T_0 to T_1, ($T_1 - T_0 = \Delta T_{1snap}$), the central segment of the unit sequence deploys while the remaining unit deformation is locked, resulting in a V-shape with a concave portion in the middle. When heated to T_2 ($T_2 - T_0 = \Delta T_{2snap}$), the encoded deformation of the other two groups of units on both sides is activated to deploy into a convex geometry, yielding an M-shape that follows the V-shape. Finally, when the temperature returns to T_0, the deployed structure resumes its initially straight configuration.

We now take a step forward and demonstrate that the units can be assembled into 2D structures capable of deploying sequentially at specified temperatures. **Figure 6**a exhibits a three-step reconfiguration through a three-by-three square lattice made up of three rows and three columns of linear units. During heating, the initial noncontact, subsequent contact, and ultimate release behavior of the units enable shape evolutions characterized by contraction followed by sequential

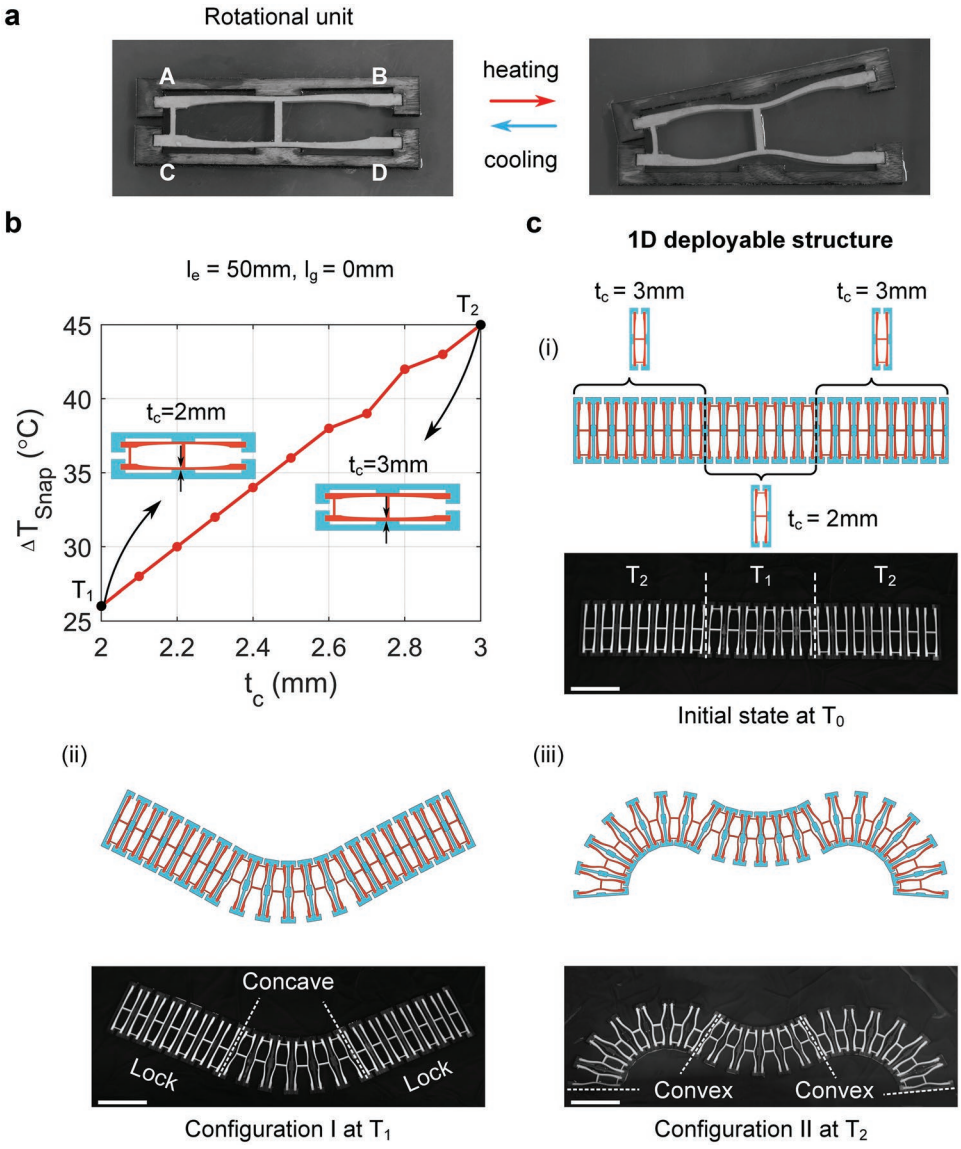

Figure 5. Rotational deformation of unit cell and thermally actuated sequential deployment at predefined temperatures. a) Rotational unit formed by joining the upper and lower beams of the core in the middle and on each side, i.e., points A,C or B, and D. The red arrow represents heating, while the blue arrow indicates cooling. b) A range of ΔT_{snap} is achieved by tailoring the core thickness, t_c, with other prescribed dimensions. c) Two-step sequential deployment of 1D structure. Rotational units with distinct ΔT_{snap} are assembled in series to form an integral lattice that is programmed to morph sequentially in response to specific temperature cues. i) Initially straight lattice at T_0 transforms into a V-shape when the middle group of the units deploys into a concave geometry at T_1 ii), while the encoded deformation of the rest remains locked. iii) At another target temperature, T_2, the concealed deformation of the lattice is activated, resulting in an M-shape that follows the V-shape. Scale bars = 108 mm.

expansion at distinct temperatures. To regulate the deploying temperature, ΔT_{snap}, and assemble the row and column units into an integral lattice, the units are assigned with identical length (L) and gap spacing (l_g), but dissimilar core thickness (t_c = 2.4 and t_c = 3 mm), and then are linked to a sub-square frame, arranged in a three-by-three square pattern. The ΔT_{snap} of the linear unit is provided in Section S6 (Supporting Information). When heated up from T_0, the lattice contracts in both X and Y directions due to the gap reduction of all units until contact is made between cores and stoppers, exhibiting negative CTEs in both X and Y directions at T_1. The experimental results reveal a dimensional reduction: $h_1 - h_2$ = 8.8 mm in the Y direction and w_1 - w_2 = 6.7 mm in the X direction. As the temperature rises further, the column units snap at T_2 and the lattice deploys in the Y direction, while the deformation of the row units remains concealed. Once the temperature reaches T_3, the locked units get activated, enabling deployment in the X direction. By returning the temperature to T_0, the framework returns back to its initially undeformed state. The experimental demonstrations illustrating the contraction and two-successive deployment over temperature can parallel the computational results.

Lastly, we demonstrate sequential deployment in multiple directions, a functionality that opens the door to multi-stage deployable structures for space applications, such as solar

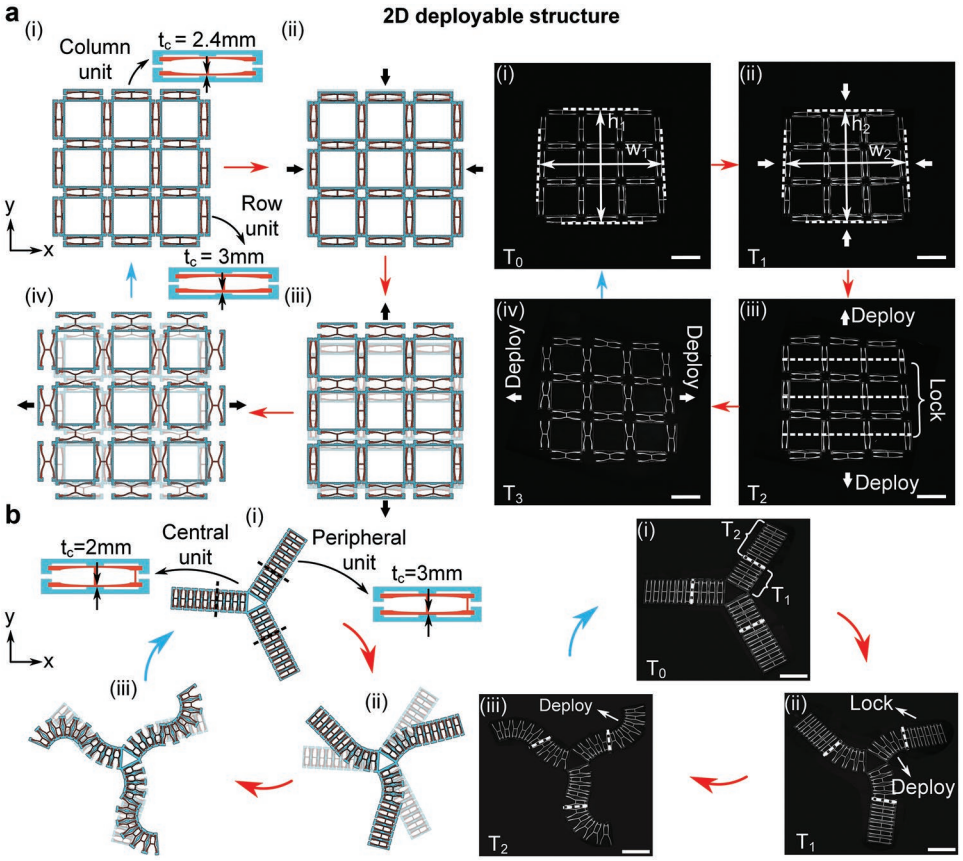

Figure 6. Thermally actuated sequential morphing of planar structure. a) Three-step deployment of a square lattice. i) A three-by-three square lattice is constructed from three rows and three columns of linear units, each with distinct ΔT_{snap}. ii) When heated from T_0 to T_1, the lattice contracts, with measured values of $h_1 - h_2 = 8.8$ mm in the Y direction and $w_1 - w_2 = 6.7$ mm in the X direction, due to the gap reduction in all units. iii) The column units are triggered to deploy in the Y direction at T_2, while the encoded deformation in the row units is concealed until the final stage of deployment at T_3. iv) Upon removal of all stimuli, the transformed lattice reverts to its original state, exhibiting reversible shape morphing. The red arrow represents heating, while the blue arrow indicates cooling. Scale bars = 116 mm. b) Sequential deployment in multiple directions for application as multi-stage deployable structures. A representative prototype of Y-shape is composed of three arms connected by a triangle frame, each consisting of two sets of rotational units with predefined ΔT_{snap}. The central units snap at T_1, whereas the peripheral ones remain inactive, causing the arms to deploy clockwise. The locked units are subsequently actuated at T_2, resulting in a counterclockwise deployment following the previous one. Scale bars = 100 mm.

arrays, and robotic arms. Here, a representative Y-shape design is examined and experimentally validated on a proof-of-concept prototype. The deployable lattice comprises three arms attached to a central triangular frame, each tessellated by two groups of rotational unit cells with distinct ΔT_{snap} (Figure 6b). Initially, the central sections rotate clockwise in response to a temperature change from T_0 to T_1, whereas the peripheral ones conceal their embedded information and await their specified cue, T_2. Once the stimulus reaches the second target temperature, the perimeter units engage and deploy in a counterclockwise fashion. The removal of the thermal stimulus enables fully reversible morphing, making it suitable for applications requiring numerous thermal cycles.

5. Conclusions

In this work, we introduce contact in thermal snapping metamaterials by leveraging the mismatched thermal deformation of the constituent materials. As a result, once contact is established during heating, the deformation can be first halted and finally reverted, resulting in a snap-through that does not need any mechanical input. Furthermore, the snapping deformation is reversible when the temperature stimulus is removed. Our analysis has unveiled the mechanism underpinning the emergence of four contact-based regimes of deformation and mapped the parameter space of the unit cell. The functionalities here investigated have been then harnessed to develop a ternary thermal switch with OFF-ON-OFF operation which differs from current thermal switches having two states only. The additional OFF state during the heating process provides another temperature threshold compared to binary switches, empowering delicate equipment in the circuit to perform an automated cutoff once overheated. By incorporating multiple units with predetermined snapping temperatures, a switch can be endowed with logic functions, capable of monitoring temperature values from multiple environment fields and governing devices in circuits to operate only within service temperature ranges.

In addition, we have presented temperature-responsive deployable structures that allow for sequential linear and

rotational deployment by tessellating a group of units encoded with prescribed ΔT_{snap}. The snapping induced deployment responsive to thermal cues does not require mechanical actuation, removing the necessity for associated actuating units such as a physical tether in a pneumatic system. No additional mechanisms are needed to deploy specific units while concealing the encoded information of the remainders. Last but not least, the morphing reversibility accomplished by our approach appeals to applications that require repeated heating/cooling cycles.

Finally, our platform is applicable to other materials and stimuli, opening up venues of application across disciplines, from space antennas, soft robots, to self-reconfigurable medical devices. For example, deployable structures constructed of metals, e.g. aluminum-titanium (Al-6061-T6 and Ti-6Al-4 V), are suitable for deploying a shelter or cover in space, where environmental temperature swings are significant and readily available.[39] Male/female connectors can be used to facilitate the assembly into 3D structures, and the fabrication method can also be extended to multimaterial additive manufacturing, provided a mismatch in material CTE is available.

Supporting Information

Supporting Information is available from the Wiley Online Library or from the author.

Acknowledgements

D.P. acknowledges the financial support of the Canada Research Chairs Program and the Natural Sciences and Engineering Research Council of Canada. L.W. acknowledges financial support from the China Scholarship Council (202006280037).

Conflict of Interest

The authors declare no conflict of interest.

Data Availability Statement

The data that support the findings of this study are available on request from the corresponding author.

Keywords

reversible thermal deformation, self-contact, sequential deployment, snap-through instability, thermal switches

Received: November 16, 2022
Revised: January 10, 2023
Published online:

[1] C. Qiao, L. Liu, D. Pasini, *Adv. Sci.* **2021**, *8*, 2100445.
[2] A. D. Marchese, C. D. Onal, D. Rus, presented at *IEEE/RSJ Int. Conf. Intell. Robot. Syst.*, San Francisco, CA, Sept., **2011**.
[3] P. Rothemund, A. Ainla, L. Belding, D. J. Preston, S. Kurihara, Z. Suo, G. M. Whitesides, *Sci. Robot.* **2018**, *3*, eaar7986.
[4] D. J. Preston, P. Rothemund, H. J. Jiang, M. P. Nemitz, J. Rawson, Z. Suo, G. M. Whitesides, *Proc. Natl. Acad. Sci. USA* **2019**, *116*, 7750.
[5] T. Mei, Z. Meng, K. Zhao, C. Q. Chen, *Nat. Commun.* **2021**, *12*, 7234.
[6] A. Rafsanjani, Y. Zhang, B. Liu, S. M. Rubinstein, K. Bertoldi, *Sci. Robot.* **2018**, *3*, eaar7555.
[7] B. Gorissen, D. Melancon, N. Vasios, M. Torbati, K. Bertoldi, *Sci. Robot.* **2020**, *5*, eabb1967.
[8] B. Haghpanah, L. Salari-Sharif, P. Pourrajab, J. Hopkins, L. Valdevit, *Adv. Mater.* **2016**, *28*, 7915.
[9] K. Bertoldi, V. Vitelli, J. Christensen, M. van Hecke, *Nat. Rev. Mater.* **2017**, *2*, 17066.
[10] T. Mullin, S. Deschanel, K. Bertoldi, M. C. Boyce, *Phys. Rev. Lett.* **2007**, *99*, 084301.
[11] K. Bertoldi, P. M. Reis, S. Willshaw, T. Mullin, *Adv. Mater.* **2010**, *22*, 361.
[12] S. Xu, Z. Yan, K. I. Jang, W. Huang, H. Fu, J. Kim, Z. Wei, M. Flavin, J. McCracken, R. Wang, A. Badea, Y. Liu, D. Xiao, G. Zhou, J. Lee, H. U. Chung, H. Cheng, W. Ren, A. Banks, X. Li, U. Paik, R. G. Nuzzo, Y. Huang, Y. Zhang, J. A. Rogers, *Science* **2015**, *347*, 154.
[13] Y. Sun, W. M. Choi, H. Jiang, Y. Y. Huang, J. A. Rogers, *Nat. Nanotechnol.* **2006**, *1*, 201.
[14] J. Shim, C. Perdigou, E. R. Chen, K. Bertoldi, P. M. Reis, *Proc. Natl. Acad. Sci. USA* **2012**, *109*, 5978.
[15] A. Rafsanjani, D. Pasini, *Extreme Mech. Lett.* **2016**, *9*, 291.
[16] S. Shan, S. H. Kang, J. R. Raney, P. Wang, L. Fang, F. Candido, J. A. Lewis, K. Bertoldi, *Adv. Mater.* **2015**, *27*, 4296.
[17] H. Yang, L. Ma, *Mater. Des.* **2020**, *188*, 108430.
[18] N. Besse, S. Rosset, J. J. Zarate, H. Shea, *Adv. Mater. Technol.* **2017**, *2*, 1700102.
[19] L. V. Elliott, E. E. Salzman, J. R. Greer, *Adv. Funct. Mater.* **2020**, *31*, 2008380.
[20] Q. Ge, A. H. Sakhaei, H. Lee, C. K. Dunn, N. X. Fang, M. L. Dunn, *Sci. Rep.* **2016**, *6*, 31110.
[21] A. Cangialosi, C. Yoon, J. Liu, Q. Huang, J. Guo, T. D. Nguyen, D. H. Gracias, R. Schulman, *Science* **2017**, *357*, 1126.
[22] J. Duan, X. Liang, K. Zhu, J. Guo, L. Zhang, *Soft Matter* **2017**, *13*, 345.
[23] D. Morales, E. Palleau, M. D. Dickey, O. D. Velev, *Soft Matter* **2014**, *10*, 1337.
[24] Y.-Y. Xiao, Z.-C. Jiang, Y. Zhao, *Adv Intell. Syst.* **2020**, *2*, 2000148.
[25] Y. Xia, G. Cedillo-Servin, R. D. Kamien, S. Yang, *Adv. Mater.* **2016**, *28*, 9637.
[26] U. Gupta, L. Qin, Y. Wang, H. Godaba, J. Zhu, *Smart Mater. Struct.* **2019**, *28*, 103002.
[27] T. Chen, O. R. Bilal, K. Shea, C. Daraio, *Proc. Natl. Acad. Sci. USA* **2018**, *115*, 5698.
[28] Y. Jiang, L. M. Korpas, J. R. Raney, *Nat. Commun.* **2019**, *10*, 128.
[29] Y. Zhang, M. Velay-Lizancos, D. Restrepo, N. D. Mankame, P. D. Zavattieri, *Matter* **2021**, *4*, 1990.
[30] J. Ding, M. van Hecke, *J. Chem. Phys.* **2022**, *156*, 204902.
[31] S. Cao, X. Chen, X. Wang, C. Han, J. J. C. J. o. V. S. Yang, *Technology* **2013**, *33*, 751.
[32] H. Heo, S. Li, H. Bao, J. Ju, *Adv. Eng. Mater.* **2019**, *21*, 1900225.
[33] V. B. Krishnan, M.S., University of Central Florida, Ann Arbor, **2004**.
[34] R. Ma, L. Liu, O. Wyman, D. Pasini, *Appl. Mater. Today* **2022**, *27*, 101432.
[35] T. Chen, H. Li, Z. Li, Q. Jin, J. Ji, *Mater. Horiz.* **2016**, *3*, 581.
[36] Y. Liu, B. Shaw, M. D. Dickey, J. Genzer, *Sci. Adv.* **2017**, *3*, e1602417.
[37] M. Y. Razzaq, M. Behl, K. Kratz, A. Lendlein, *Adv. Mater.* **2013**, *25*, 5514.
[38] Y. Mao, K. Yu, M. S. Isakov, J. Wu, M. L. Dunn, H. J. Qi, *Sci. Rep.* **2015**, *5*, 13616.
[39] S. Taniker, P. Celli, D. Pasini, D. C. Hofmann, C. Daraio, *Int. J. Solids Struct.* **2020**, *190*, 22.